Trans. JWRI, Vol. 26 (1997), No. 1

# Short-circuiting Transient Phenomena in GMA/$CO_2$ Welding † (I)

## - Through-the-Wire Sensor for Feedback Torch Height Control -

**Peter ORSZAGH*, You Chul KIM** and Kohsuke HORIKAWA*****

**Abstract**

*The GMAW process with short-circuit metal transfer was investigated with the aim of defining an appropriate parameter for torch-to-workpiece distance monitoring in real time. A high speed data acquisition system was designed for current and voltage waveform sampling. A PC based analyser was used for post process data analysis to study the arc and short circuit state of the process. Transient phenomena related to liquid bridge profile changes were studied by means of simulated homophase drop-pool "touching" experiments. The time dependency of contact radius spreading and neck formation in the short-circuit stage of the welding process were analysed. It was found that torch-to-workpiece distance can be reliably detected from wire resistance during short-circuit stage of the welding process. This distance can be measured up to 100 times a second, which enables the signal to be used as a "through-the-wire" sensor for seam tracking in GMAW with short-circuiting metal transfer mode. The sensor was tested under various welding parameters and its applicability was confirmed by real time monitoring of the sensor signal.*

**KEY WORDS :** (GMA Welding) (Short-circuit) (Metal Transfer) (Liquid Bridge) (Drop Profile) (Position Sensor) (Seam Tracking)

## 1. Introduction

Due to fierce world-wide economic competition, the industrial sector is investigating every possible means to improve the efficiency and the quality of its manufacturing processes, including welding. Welding operations represents more than 40% of all manufacturing activities and among the arc welding processes, gas metal arc welding process (GMAW) is the most frequently used in practice. A combination of high process applicability on one side and extremely rash welding environments on the other side, GMAW creates a very great potential for applications of robots and mechanised systems. It is obvious that automatic welding systems can better address problems related to weld quality, repeatability, productivity, effectiveness, three shift operation, health and safety requirements, shortage of skilled welders, etc. However, many technical aspects and engineering problems are involved in arc welding automation and so there is no general and simple solution available on the market at present.

One of the basic hurdles in GMAW automation is insufficient flexible adaptation of the welding system to a huge variety of joint geometries, welding trajectories, torch-to-workpiece positions and orientations. Weld joint detection and seam tracking functions represent basic and imperative features of automatic welding systems. Small, inexpensive, reliable and precise torch-to-workpiece position sensors, which are capable of coping with extremely rash welding environments, become crucial elements for flexible automation and robotisation of arc welding processes in this way.

The paper describes results, which have been achieved in the development of a new type of welding torch position sensor. The new sensor enables a real-time measurement of the torch-to-workpiece position in GMA welding with short-circuiting metal transfer. The sensor is based on a unique detection algorithm, which detects the torch-to-workpiece distance from welding current and voltage waveforms, regardless of large variations in welding parameters. The sensor was tested with various welding parameters and conditions.

† Received on May 19,1997
* Visiting Scientist, Slovak Technical University
** Associate Professor
*** Professor

Transactions of JWRI is published by Joining and Welding Reseach Institute of Osaka University, Ibaraki, Osaka 567, Japan.

## 2. Seam tracking and adaptive welding

**Figure 1** shows basic classification of a control block in welding systems. The systems of the first 2 levels are mostly used in practice. According the classification, welding systems equipped with seam tracking functions fall in the 2nd level. They are characterised by a stabilisation of process input variables (X) in order to reduce the effect of random perturbations (W) on the final quality of the welds (Y). This level includes stabilisation of welding parameters[1-3] (current, voltage, wire feed rate, welding speed, etc.) and torch-to-workpiece relative position[4,5] using real-time feedback control loops.

Typical perturbations affecting the torch-to-workpiece position are mostly generated in operations prior to welding. They are defined by dimensional variations of welded parts, such as weld parts and weld bevels tolerances, inaccuracy of weld parts positioning and workpiece fixing, errors in torch path programming, etc. Some perturbations occur during the welding operation, e.g. position changes due to thermal deformations, residual stress relief, etc. If the harmful effect of perturbations is too significant, an unacceptable low weld quality is observed. It results in an operator's corrections of welding parameters during welding or/and the welding operation has to be interrupted.

For the past 30 years various types of position sensors have been developed for arc welding and some of them have been used in industrial manufacturing. One can find one/two dimensional contact probe sensors[6-8] with or without memory delay playback function, electrode contact sensors[9,10], electromagnetic sensors[11], arc sensors[12-16], optical sensors[17-21], sound sensors[22], etc. Excellent reviews of the sensors, and their industrial applications in arc welding processes can be found in literature[11,22].

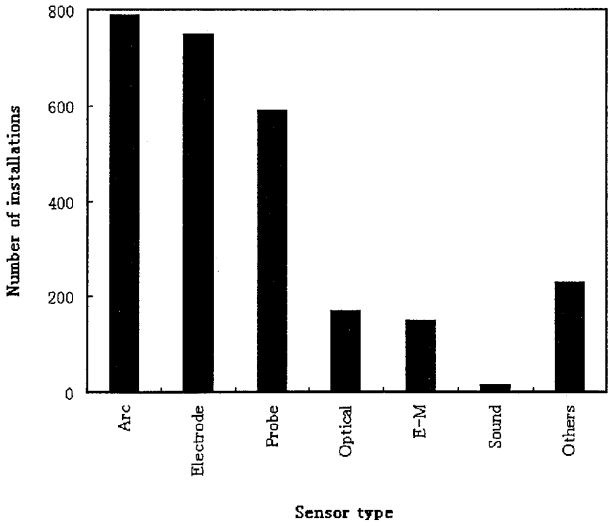


**Fig. 2** Sensors used in arc welding[22]

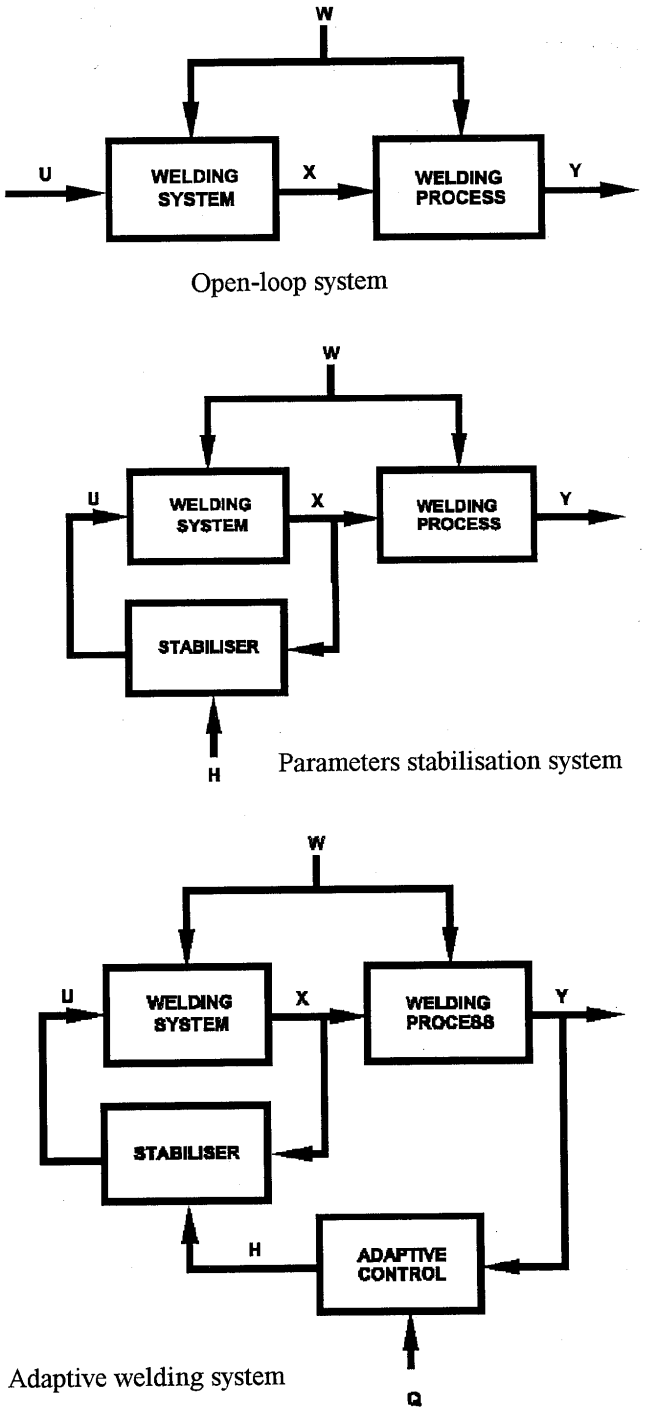


**Fig. 1** Control systems in welding processes

Both reviews show that only contact (probe and electrode type) and arc sensors are widely used in welding practice. **Figure 2** shows the number of sensor installations in arc welding applications. The arc sensors, due to their advantages (such as measurement and arc position coincidence, real time control capability, no space requirements in the weld pool vicinity, low installation and maintenance cost, etc.)

**Table 1** Welding parameters and conditions

| Parameter | Description | Value |
|---|---|---|
| Base material | Mild steel | 500x100x12 mm |
| Wire material | Mild steel MIX-50S, Stainless steel YT-308L | ∅ 0.8, 1.2, 1.6 mm |
| Welding speed[1] | Range | 1 to 25 mm/s |
| Torch height | Range | 11 to 30 mm |
| Wire feeding[2] | Rate | 2 to 25 m/min |
| Shielding gas | Ar, CO2, MIX(80%CO2+20%Ar) | 15 l/min |
| Test | Bead on plate | 20 s |
| Welding voltage[3] | Range<br>Static voltage drop | 15 to 29 V<br>0 to 5 V/100A |
| Welding current | Range<br>Dynamic short-circuit current rise | 0 to 800A<br>50 to 240 kA/s |

[1] *Carriage type : CR-64* [2] *Feeder type : MLWH-232* [3] *Power source type : Transistarc 800*

are especially desirable for seam tracking and adaptive welding control systems. Arc sensors, based on the arc length feedback control by means of AVC or ACC principles, are primarily used in GTAW, GMAW with spray metal transfer mode and plasma welding and cutting.

In GMAW with short-circuit metal transfer modes, especially in GMAW with $CO_2$ shielding gas, arc sensor applications are very limited[23]. A short-circuit metal transfer mode with its extreme variations of instant welding parameters strictly limits sensitivity and torch-to-workpiece position detection characteristics of the sensor. Some attemps[24,25] to use the arc sensor for seam tracking in GMAW/$CO_2$ have been carried out, but they are still in the R&D stage.

## 3. Experimental techniques and materials

### 3.1 Welding experiments

GMAW experiments were carried out in the horizontal position. A series of single pass beads on plate were deposited at constant welding speed under various welding parameters and conditions. The plate material and welding wire were of mild steel and stainless steel. Three kinds of shielding gas were used.

The experimental welding set-up is shown in **Fig. 3**. The torch was stationary, fixed to a motorised vertical support, which enabled the torch-to-workpiece position to be changed. The plates were attached to a welding carriage, which moved the plates at a constant welding speed. A transistorised welding power source of the analogue type was used. Its adjustable static output characteristics were set from CP (constant potential) to CC mode (constant current). Most tests were carried out with a slightly drooping characteristic. Dynamic parameters of the power source were pre-set by an electronic reactor, which determined a short-circuit current waveform (ramp).

**Table 2** Data acquisition parameters

| Parameter[1] | Value |
|---|---|
| Scan | 2 channels |
| Scanning period | 20 μs |
| Scanning mode | Burst |
| Trigger | Internal |
| Data volume | $2x10^6$ |
| Data transfer | DMA |
| Sampling activity | 20 s |
| Acquisition control | DAP95 |
| Data analyser | ANA95 |

[1] *System type : DAS-1801*

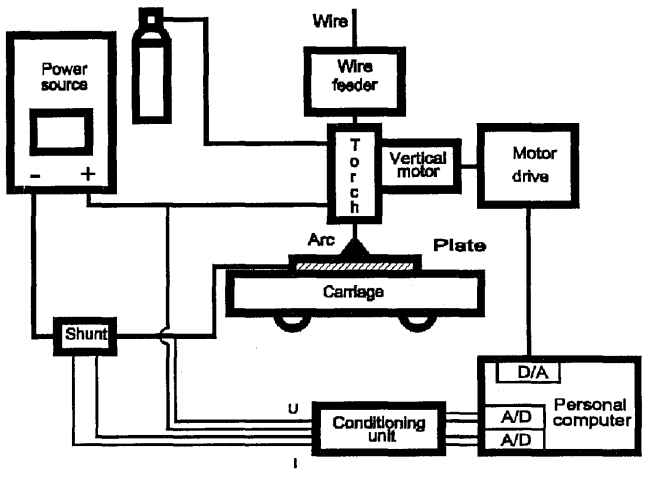


**Fig. 3** Experimental welding set-up

During the tests, welding current and voltage were monitored by high speed data acquisition systems and data were transferred to files for post-process analysis. Parameters of welding experiments are summarised in **Table 1** and **Table 2**.

### 3.2 Homophase drop-pool "touching" simulations

To study bridging phenomena in short-circuit GMAW, simulated drop-pool "touching" experiments were carried out first and digital high speed photography was used for recording transient drop/bridge profiles. The experimental set-up used in the experiments is shown in **Fig. 4**.

Pendant drops were formed on a solid steel rod with a flat bottom tip surface. The rod was smoothly moved downwards until the drops touched the pool surface of the container with a liquid. In experiments with mercury the drops were created by means of a injection method. Vertical movement of the rod was precisely controlled by a computer and a slow approaching speed 0.32 mm/s was used in all experiments. To reduce shaking of the apparatus in the vicinity of the pool surface the support liner and the working table with the liquid container were mechanically fixed each other in order to create a compact structure. The structure was attached to a stable rigid steel frame by means of soft flexible suspensions. The volume of the liquid in the container was precisely set so that the pool surface reached the height of the apparatus's optical axis. A diameter of the container was 5, 10 and 30 mm.

High speed digital photography with backlighting technique was used for recording transient bridging phenomena. The movies were recorded in camera memory and transferred to a computer afterwards. The whole picture sequence - from the beginning (a touching contact development) up to the end (a liquid bridge breakage or a stable meniscus) - was analysed by means of special software. For automatic drop/bridge profile recognition, several digital image processing techniques, such as pixel intensity filtering, picture smoothing and image enhancement and restoration[26,27], were applied.

Experiments were carried out with various solid steel wire rods, of different diameters, several kinds of liquid and drop volumes (heights). Only homophase drop-pool bridging phenomena were studied. Four liquids with significantly different physical properties, e.g. mass density, surface tension, contact angle and kinematic viscosity were selected. The values were mostly taken

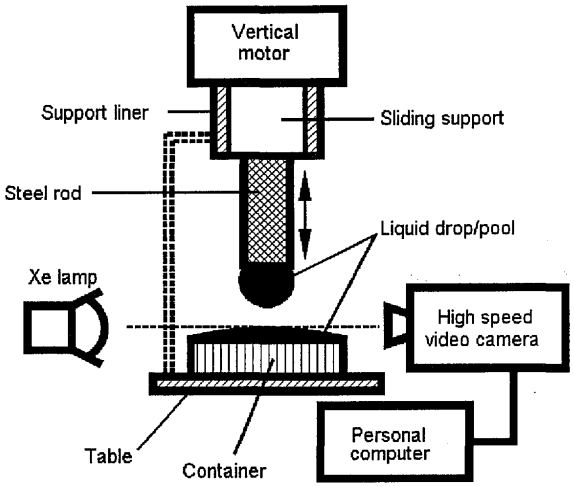


**Fig. 4** Apparatus for simulated "touching" tests

from the literature for pure materials, some values were directly measured or calculated from experimental data. The data of the liquids used in experiments are summarised in **Table 3.**

## 4. Results and discussion

### 4.1 Current and voltage waveforms

In the GMAW process a welding power source usually has a constant voltage or slightly drooping static characteristics. The main reason for the CP static mode is a natural self-regulation of arc length and a compensation of torch-to-workpiece distance variations. The self-regulation is carried out by means of current increase/decrease whenever the torch to-workpiece distance decreases/increases.

In contrast with GMAW with a spray metal transfer mode, in the GMAW/$CO_2$ process the arc does not burn continuously, but it is erratically interrupted by short circuiting. **Figure 5** shows typical waveforms of instant current and voltage values in 3 different time zoom scales (1x, 100x and 500x). Top graphs also show average values of welding parameters.

**Table 3** Physical properties of liquids used in simulated experiments

| **Liquid type** | **Mass density** *(kg/m³)* | **Surface tension** *($10^{-3}$N/m)* | **Contact angle**[1] *(deg)* | **Typical length**[2] *(mm)* |
|---|---|---|---|---|
| Water | 1 000 | 73 | 60* | 2.72 |
| Ethyl | 820* | 22 | 0 | 1.65 |
| Oil | 921* | 29* | 0 | 1.79 |
| Mercury | 13 546 | 475 | 120 | 1.89 |
| Iron[+] | 7 000 | 1 200 | 0 | 4.18 |

[+] *liquid iron added* * *measured value* [1] *liquid/steel pair* [2] $L_t = (\sigma/\rho/g)^{1/2}$

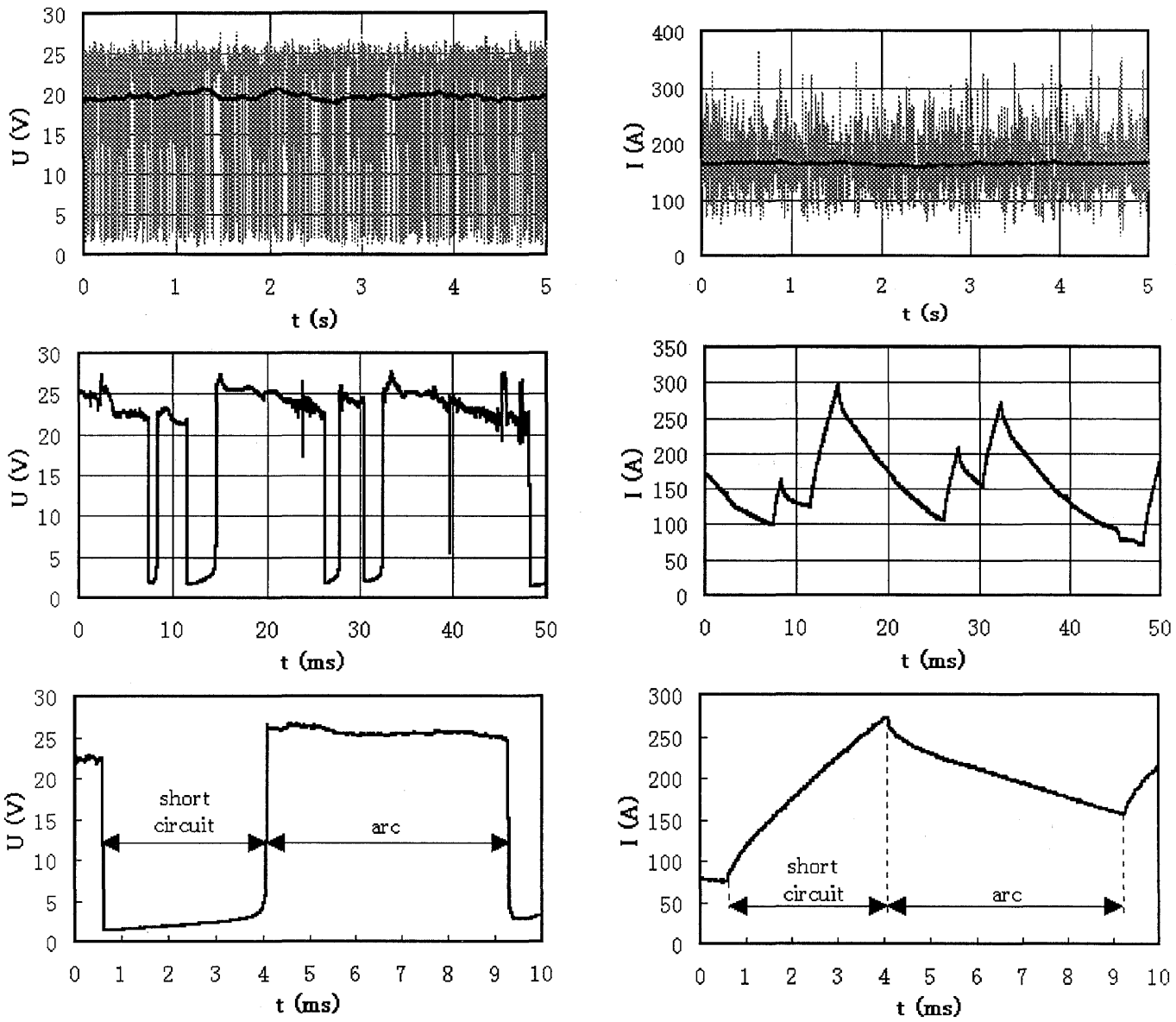


**Fig. 5** Typical current and voltage waveforms in GMAW/$CO_2$ with short-circuit metal transfer mode
*(I=165A, U=20V, $v_d$=4m/min, L=14mm, MS wire ∅1.2 mm, CP mode, $K_I$=60kA/s)*

In the arc burning stage, the electrode tip is melted mostly by arc and Joule heating and a liquid drop is formed at the tip of the wire. The drop gradually grows and moves to the weld pool. The arc length decreases in this way and the current decreases by discharging of a power reactor.

When the liquid drop becomes large enough to reach the weld pool it touches the pool surface and the arc is extinguished. A short-circuiting liquid bridge is created between the wire and the workpiece. Low voltage values voltage values can be detected and a rapid short-circuit current ramp is generated, limited by the pre-set dynamic current slope of the welding power source. After drop-pool contact is created a liquid bridge profile (**Fig. 6**) is

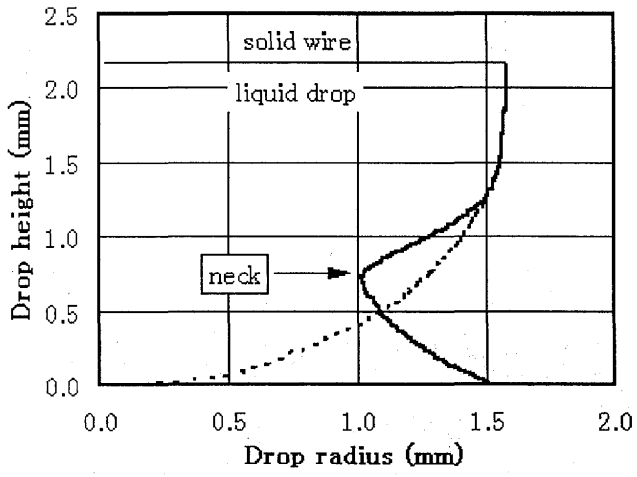


**Fig. 6** Drop-pool liquid bridge profile (water simulation)
--- initial drop profile, — neck formation after 4 ms

mainly controlled by capillary and electromagnetic forces. Their combined effect will result in a neck formation in the liquid bridge. The neck gradually becomes narrower due to a increasing squeezing action of the electromagnetic force, generated by the rapid welding current ramp. At the end of the short-circuiting stage the liquid bridge breaks in the neck location and the arc is instantly re-ignited in the gap between the electrodes.

### 4.2 Process basic statistics

GMAW with short-circuiting metal transfer mode is characterised by fast alternation of arc burning and short-circuiting state. The welding parameters show tremendous ripples, which directly prevent the extraction of torch-to-workpiece distance information from measured signals by means of standard "arc sensor" techniques or by filtering or moving-average methods. Due to fundamental differences between the arc burning and short-circuiting stages both current and voltage waveforms were separately analysed in arc burning and short-circuiting stages.

In the arc burning stage the arc length and the wire extension do not reach quasistationary balance as in GMAW with spray metal transfer mode. Both parameters dynamically change at the rate of short-circuiting frequency. When flat or slightly falling static characteristics of the power source are used, both the arc current and the wire extension vary extensively during the arc burning stage in order to reach the process self-regulation balance conditions. However, the wire feeding rate is always higher than the wire melting rate and the arc length is gradually decreased until the liquid drop at the wire tip touches the molten pool surface. A liquid bridge is formed between the wire and the molten pool and homophase drop-pool touching phenomena with transient liquid bridge profile can be observed.

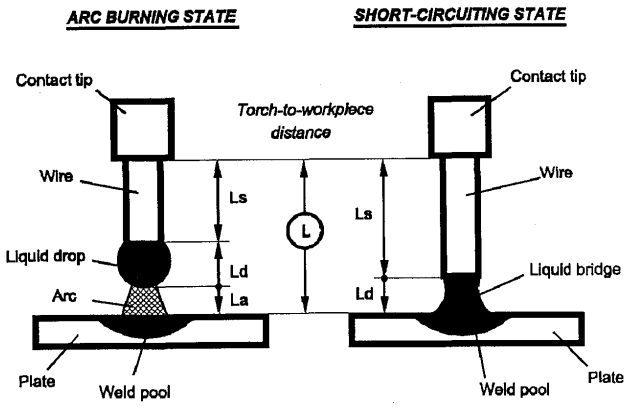


**Fig. 7** Torch-to-workpiece configuration

**Figure 7** shows the torch-to-workpiece configuration. In the arc burning stage the torch height $L$ is divided into 3 sections : solid wire length $L_s$, liquid drop length $L_d$, and arc length $L_a$. All the parameters are not stable and they change during the arc burning stage due to the combined effects of different wire feeding/melting rate and the drop growth. Mutual solid wire length, drop length and arc length variations occur in every arc burning cycle regardless of constant total torch-to-workpiece distance L. For mild steel wire, ∅1.2mm, and $CO_2$ shielding gas, typical values of arc duration are from 3 ms to 12 ms (see **Fig. 8**). The arc burning duration depends significantly on pre-set welding parameters and conditions (see **Fig. 9**).

During the short-circuit stage the welding wire comes to direct contact with the molten pool and the arc is extinguished. At this moment the wire extension $L_e$ becomes equal to the torch-to-workpiece distance $L$. The distance has 2 sections : solid wire length $L_s$ and liquid drop length $L_d$. During short-circuiting stage both wire and drop length can vary from one short-circuit to another, due to drop size variations, caused by different arc burning durations in the process. For mild steel wire, ∅1.2mm, typical values of short-circuiting durations are 0.5 - 3.5 ms and short-circuiting frequency is about 40-100 Hz.

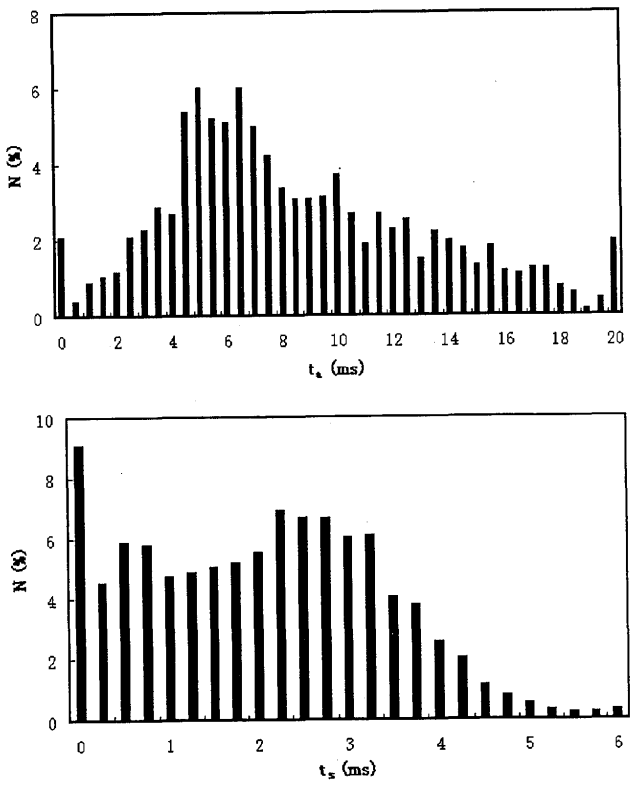


**Fig. 8** Distribution of arc burning duration ($t_a$) and short-circuiting duration ($t_s$) in GMAW/$CO_2$
*(I=165A, U=20V, $v_d$=4m/min, L=14mm, MS wire ∅1.2 mm, CP mode, $K_I$=60kA/s)*

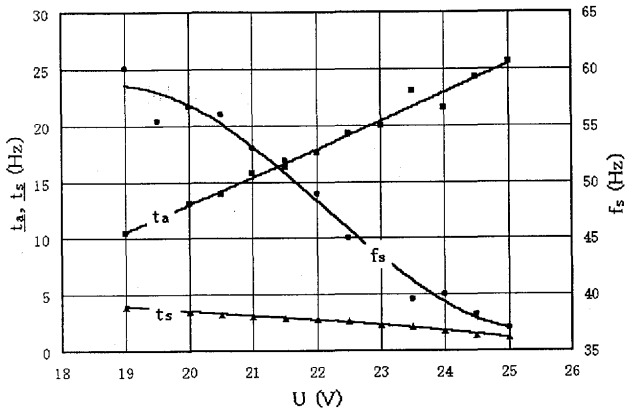


Fig. 9 Dependence of arc burning duration ($t_a$), short-circuiting duration ($t_s$) and frequency ($f_s$) on welding voltage (U) *(I=190A, U=19-25V, $v_d$=5.2m/min, L=14mm, MS wire ∅1.2 mm, CP mode, $K_I$=60kA/s)*

Both parameters (duration and frequency) depend on pre-set welding parameters and conditions.

In the GMAW/$CO_2$ process the arc erratically changes length from its maximum value to zero, when it is extinguished by short-circuiting metal transfer. Due to the alternation of arc burning and short-circuiting stages both current and voltage waveforms show huge natural ripples. It is difficult to filter them out to get a stable signal with torch-to-workpiece information for feedback torch position control in seam tracking systems. Moreover, the short-circuiting frequency range (40-100Hz) is close to a rotation frequency of the torch in HSRA systems. These are the reasons why dynamic arc length variations prevent the use of instant arc parameters for reliable torch height detection and feedback control.

Keeping all this in mind the process analysis focused on the short-circuiting stage with the major objectives : how to detect the wire extension *($L_e$=L)*, what kind of signals to measure, how/when to sample data and how to extract the desired position information from the measured data ?

### 4.3 Short-circuiting phenomena monitor

The easiest way to measure the wire length by means of electrical methods is to measure its resistance. Knowing the resistance of the wire the length can be calculated from formula :

$$R=\frac{\xi L}{S} \qquad (1)$$

However, during the welding process the wire is heated by Joule energy and by the arc during the arc

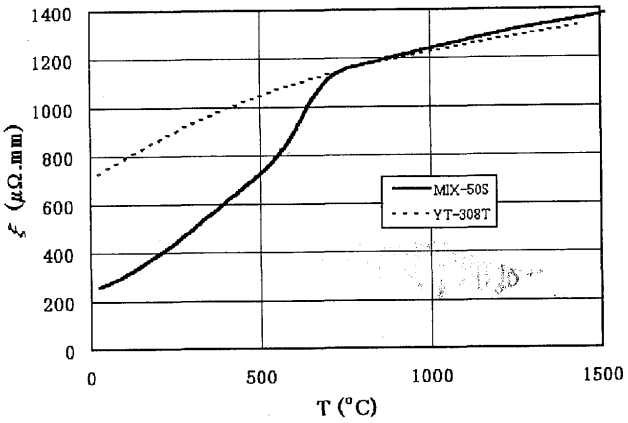


Fig 10 Resistivity ($\xi$) of mild and stainless steel[28] (MS : MIX-50S, SS : YT-308T)

burning stage. As the resistivity $\xi$ of mild steel strongly depends on temperature $T$ (see **Fig. 10**), the total wire resistance will depend on temperature distribution $T(z,t)$ in the wire. Detailed analysis of temperature distribution (transient and quasistationary temperatures) in the moving wire in GMAW can be found in the literature[29].

It is obvious from Eq.(1) that the wire resistance, $R$, strongly depends on the wire cross section, $S$, or the wire radius, $(\sim 1/r^2)$. As the liquid bridge profile is not constant during the short-circuiting state the cross section, $S(z,t)$, of the bridge will depend on time, $t$ and wire location $z$.

Due to wire heating and liquid cross section variations, the total wire resistance $R$ in the short-circuiting state will depend on time $t$ and be calculated from the integral formula :

$$R(t)=\int_0^L \frac{\xi(T(z,t))}{S(z,t)}dz \qquad (2)$$

**Figure 11** shows typical waveforms of welding current and voltage during the first short-circuit at the start of the welding process. A liquid drop-pool touch event at the beginning of the short-circuit was detected at $t\approx 10$ *ms*. The end of the short-circuit, when the liquid bridge was broken, was found to occur $t\approx 43$ *ms*. The first short-circuiting stage lasted $t_s\approx 33$ *ms*. It can be seen from the graph that during the short-circuiting stage the current rapidly increased from 0A to maximum power source current level 800A. The maximum was reached very fast in about 20 ms. The current ramp slope at the beginning of the short-circuit was 192 kA/s.

When welding current and voltage values are known, the welding resistance can be determined from the measured data. On the other hand, the resistance of the wire can be calculated theoretically from the numerical model by means of Eq.(2), when temperature distribution

$T(z,t)$, liquid bridge profile $S(z,t)$ and resistivity $\xi(T)$ are known. The data required for the calculation and the current waveform in Fig. 11 were taken from Ref.[29].

The result is shown in **Fig. 12.** The graph shows two waveforms during the first short-circuit : *(m)* measured total welding resistance and *(c)* calculated wire resistance. Both curves are shown as functions of time.

It can be seen from the graph that both curves show similar behaviour, except at the beginning and the end of the short-circuiting stage. At the start point ($t \approx 10$ *ms*) the cold wire comes into contact with the cold surface of the workpiece. As the tip of the wire is not ideally flat a contact area between the wire tip and a workpiece surface is smaller than the wire cross-section. Microscopic contact-bridges are created first and the total welding resistance is very high(>200mΩ). The wire feeding increases pressure in the contact location and gradual melting of small contacts leads to a electrical breakdown of contact surface films. As the current is low at the beginning, wire heating is not very intensive. Total resistance decreases following the spreading of contact radius and eventually the initial process will result in full cross-section contact formation. Figure 12 shows that the contact formation stage took about 4 ms *(10<t<14ms)*.

After the contacting stage both curves show the same trend. The centre part of the curves *(14<t<35ms)* represents the wire heating stage. The resistance increase is caused by wire heating only due to Joule energy dissipation. The absolute difference between the curves in the centre part of the curves indicates the value of ballast resistance in the measurement circuit (e.g. contact resistance between the electric tip and the welding wire,

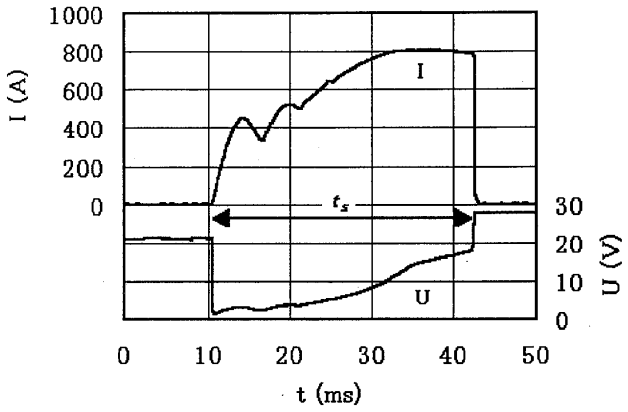


**Fig. 11** Welding parameters at the start of GMAW process *($CO_2$, ∅1.2mm, MS, L=17mm, $v_d$=5.2m/min, $K_I$=60kA/s, CP mode)*

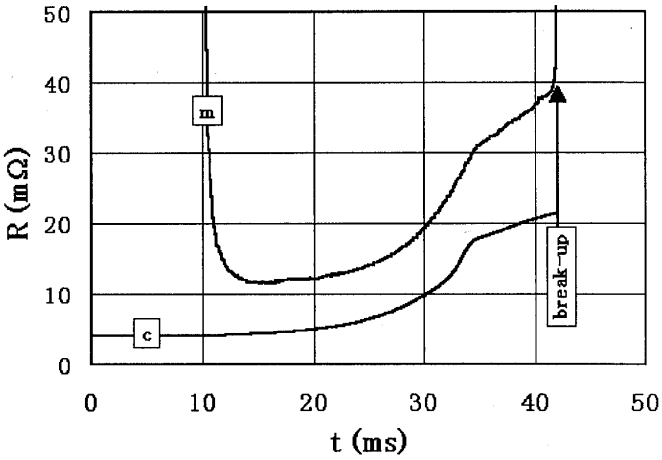


**Fig. 12** Resistance waveform at the start of GMAW process
m - measured welding resistance c - calculated wire resistance
*($CO_2$, ∅1.2mm, MS, L=17mm, $v_d$=5.2m/min, $K_I$=60kA/s, CP mode)*

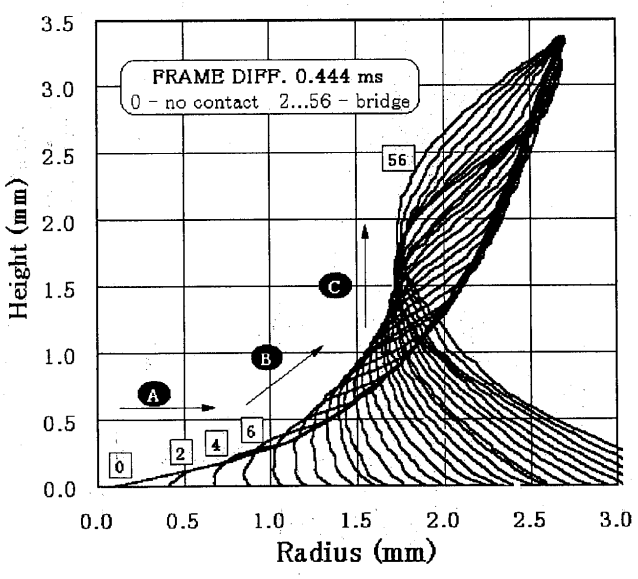


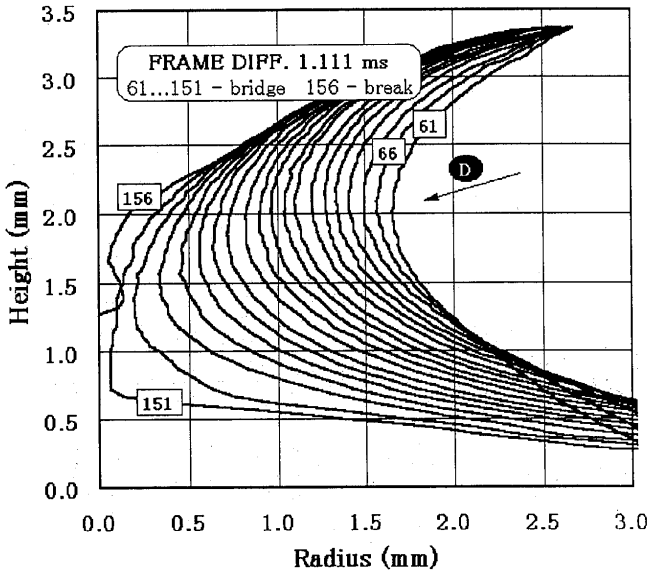


**Fig. 13** Liquid bridge profile development (homophase water simulation)
(Break-up time 34 ms, drop volume 46.5 $mm^3$)

resistance between the welding torch and measurement point, etc.). Parallel curves indicate that after electrical breakdown of surface films the ballast resistance is usually independent on time and current. This is in good agreement with Ref.[30,31].

In the last stage of the short-circuit the current level is very high. The wire heating becomes very intensive due to a high resistivity of the wire and a high current level. A liquid bridge profile with a neck is formed between the solid wire and the plate. With the high current and the neck profile of the bridge the liquid is rapidly squeezed by radial electromagnetic forces (pinch effect). The resistance increases due to both effects, the intensive wire heating and the neck cross-section reduction. The measured welding resistance shows a steeper increase than the calculated curve, which includes the wire heating only.

In GMAW with short-circuiting metal transfer mode a liquid drop touches a weld pool surface and transient liquid bridge profile can be observed. Homophase liquid touching phenomena were studied in simulated experiments. **Figure 13** shows typical liquid bridge profile development, when a liquid drop touches a pool surface of the same kind of liquid (homophase drop-pool touching). Time resolution was 222 μs. It can be seen from the left picture that in the first stage a fast contact radius spreading is the dominant process. Apart from the region close to the pool, the liquid drop does not move and the bridge does not change profile. At the beginning of the stage the total resistance of the bridge is high due to a very small contact area between the drop and the pool. As the contact area becomes wider the resistance decreases.

**Figure 14** shows the resistance of the bridge as a function of time. A sharp drop of resistance is well-marked at the beginning of the graph. The curve behaviour in this stage expresses the contacting process between the drop and the pool *(t<5ms)*, when fast radial contact spreading occurs on the surface of the pool (arrows A and B in Fig.13). During the first contacting stage the resistance of the liquid bridge has a negative first derivative *(dR/dt<0)*.

The centre part *(5<t<15 ms)* of the resistance shows a relatively flat plateau, indicating a small change of the resistance. During this stage the neck radius is not significantly changed. It only moves up from the pool vicinity closer to the solid wire tip (arrow C in Fig.13). The resistance of the bridge is almost constant, because it depends on the neck radius, not on the neck position within the bridge. Therefore the second stage of the bridging is characterised by the first derivative of the bridge resistance close to zero *(dR/dt≈0)*.

In the last stage of bridging, the liquid bridge is gradually squeezed by capillary forces (arrow D in Fig. 13) and the neck radius decreases. The narrower the neck is, the higher the resistance of the bridge becomes. During the squeezing stage *(t>15 ms)* the resistance increases and the curve has a positive first derivative *dR/dt >0*.

As it can be seen from the graph in Fig.14 the resistance curve is not symmetric. The absolute value of the first derivative is higher in the contacting stage than that in the squeezing stage. The trend of the curve indirectly indicates that the contact radius spreading was a faster process than the squeezing of the neck. The same behaviour was observed in most simulated experiments, regardless of liquid type (ethyl, water, oil, mercury), initial drop volume and solid wire radius in the range from 1.2 to 5.9 mm.

Physical properties and drop sizes of different tested liquids had small effects on contact radius spreading speeds. **Figure 15** shows typical patterns of contact spreading and neck formation in homophase drop-pool bridging in simulated experiments.

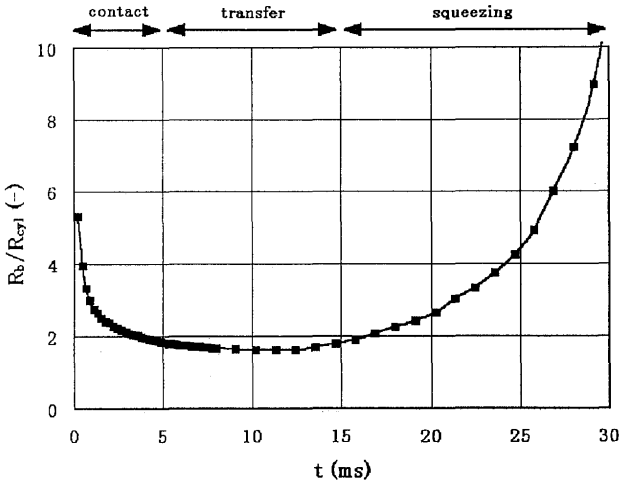


**Fig.14** Resistance of the liquid bridge
(water simulation in Fig.13)
$R_d$ - resistance of the bridge
$R_c$ - resistance of equivalent cylinder ( $r=r_w$)

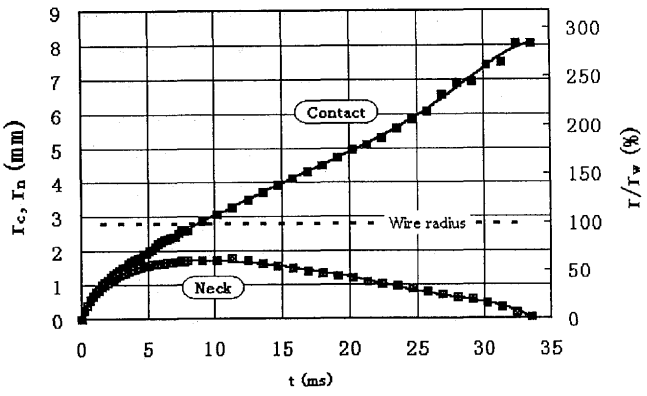


**Fig.15** Contact spreading and neck formation
(water simulation in Fig.13)
$r_c$-contact radius $r_n$-neck radius $r_w$-wire radius

The contact radius expands very rapidly in the first several hundred microseconds. The initial radial contact spreading speed reached up to 1 m/s. During the contacting stage the drop-pool contact region represents the narrowest part of the bridge with the highest resistance. After rapid radial expansion the contact spreading continues at slower speed until the contact reaches the pool boundary of the container.

Shortly after the stable drop-pool contact is formed the neck appears just above the pool surface. From this moment the narrowest part of the bridge does not coincide with the contact region any more. The contact-neck separation occurs very quickly after the drop touches the pool surface (see detail in **Fig.16**). The typical contact-neck separation time (≈1ms) was observed in all simulated experiments, regardless of liquid surface tension, density and drop size.

Physical properties of liquids, such as surface tension, density, viscosity) had a significant effect mainly on the second (transfer) stage. The higher the viscosity and the drop size were the longer flat plateau was observed. A smaller effect was found on The squeezing stage duration. A very small effect was observed on contacting duration and contact spreading speed.

During the contacting stage the contact region represents the region with the highest resistance and so total bridge resistance changes will closely correspond to the contact radius variations. Similarly, in the squeezing stage, the total resistance curve will follow the neck profile variations.

**Figure 17** shows the liquid transfer from the drop to the pool at various moments after homophase drop-pool touching. The transferred volume is defined as the volume below the neck. It is obvious that in the first moments *(t<1ms)* almost no liquid is transferred. The drop profile is not changed, except in a very small region close to the pool surface. Only a rapid radial contact spreading occurs. However, in the centre stage *(2<t<15ms)* the liquid transfer is very intensive and most of volume is transferred below the neck. In the last squeezing stage of the bridging the volume below the neck is practically unchanged. The total transferred volume of the liquid from the drop to the pool is about 80% of initial drop volume. Experiments with different liquids and drop sizes show very similar results, as far as the S-shape of the transfer curve, initial transfer delay (≈1ms), rapid transfer speed in the centre part, slow transfer rate in the last squeezing stage and the total transferred volume (≈80%) of the initial liquid drop size, are concerned.

In GMAW with low welding parameters, the arc burning is erratically interrupted by the short-circuiting metal transfer. The welding electrodes (wire and workpiece) come into direct contact and so homophase drop-pool touching phenomena, described above, occur during every short-circuit. **Figure 18** shows measured waveforms of welding resistance in several sequential short-circuits. The arc burning cycles were removed from

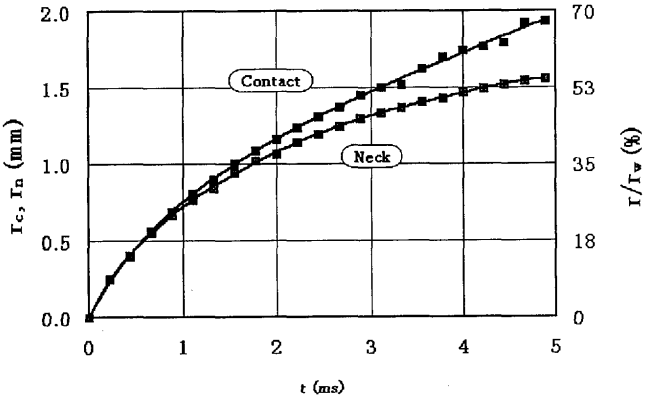


**Fig.16** Detail of contact spreading and neck formation at the contacting stage (water simulation in Fig.13)
$r_c$-contact radius $r_n$-neck radius $r_w$-wire radius

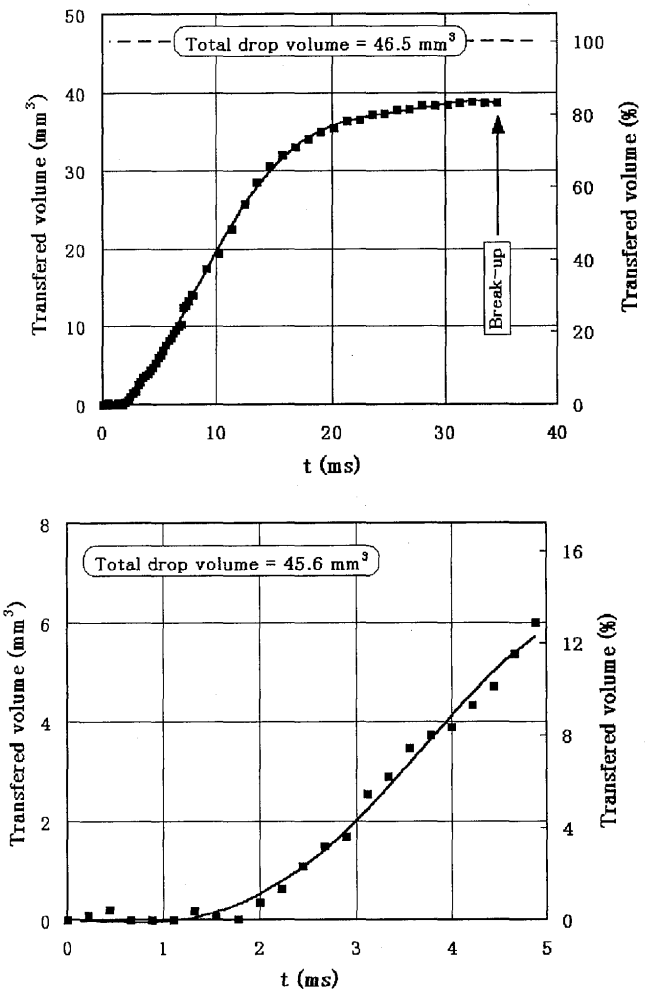


**Fig.17** Drop-to-pool liquid transfer (water simulation)

the data. Detail of the 2nd short-circuit can be seen in **Fig. 19**, where a 2.5x time zoom scale is applied.

It is obvious from the graphs that the resistance curve has a typical U-shape, which is characteristic for homophase liquid drop-pool "touching" phenomena (see Fig.14). At the beginning of the short-circuit the resistance falls very rapidly following the drop-pool contact radial expansion just above the weld pool surface. From Fig. 19 it can be seen that the fast contact spreading lasted only about ≈1.3 ms *(0.7<t<2ms)* and after a very short flat plateau ≈0.5 ms *(2<t<2.5ms)* the resistance started to rise *(t>2.5ms)*, indicating the beginning of the neck squeezing stage. The whole metal transfer lasted about 3 ms. After the short contacting stage (resistance fall) with neck formation, the neck was almost immediately squeezed by the electromagnetic force, governed by welding current level $I$. As the short-circuit current ramp is very steep (see Fig. 5) and the electromagnetic force depends on current ($\sim I^2$), the squeezing process takes place much faster than the one in simulated experiments, in which the squeezing process was governed by capillary and gravity force only (no current flowing through the bridge). However, three typical stages of the drop-pool homophase touching with a liquid transfer (A-contact spreading, B-liquid transfer below the neck and C-neck squeezing) can be clearly recognized from the welding resistance. Welding resistance with the characteristic U-type shape waveform during a short-circuiting state can be used as a reliable real-time short-circuiting phenomena monitor in GMAW with short-circuiting metal transfer mode. This signal is also used for a torch-to-workpiece distance detection by means of a new position sensor.

### 4.4 Principle of the through-the-wire sensor

Taking into account characteristics of homophase drop-pool touching phenomena a new detection method of the torch-to-workpiece distance can be proposed as follows. In the short-circuiting stage the torch-to-workpiece distance corresponds to the wire extension. The wire extension (length) can be determined by measurement of its resistance, when the wire is in a good electrical contact with the weld pool.

To avoid a high resistance of the drop-pool contact region at the beginning of the short-circuit the resistance should be sampled after the contact radius is wide enough *(t>1ms)*. The contribution of the contact region to the total welding resistance will be reduced in this way and the measured value will better correspond to the torch-to-workpiece distance $L$.

On the other hand the welding resistance can not be measured too late. At the end of the short-circuiting stage the resistance becomes high again. In the squeezing stage of the short-circuit the neck region is developed and the neck becomes very narrow.

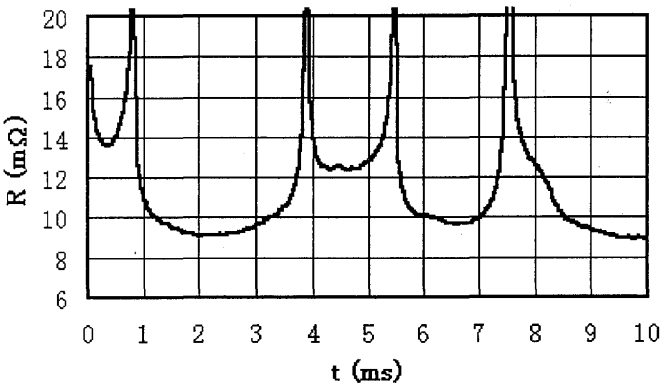


**Fig. 18** Typical resistance waveforms in short-circuiting state (arc burning state removed)
*(I=190A, $v_d$=5.2m/min, L=14mm, MS wire Ø1.2 mm, CP mode, $K_I$=60kA/s)*

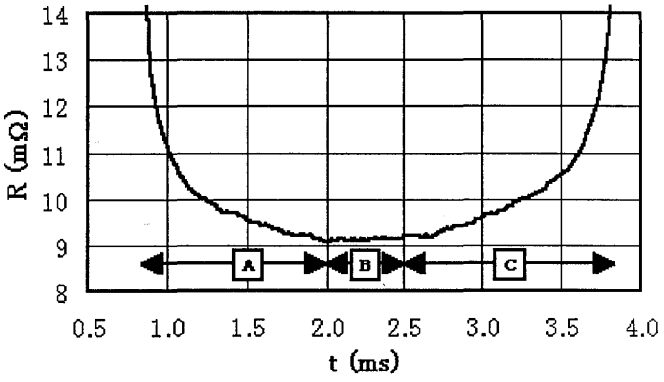


**Fig. 19** Detail of resistance waveform in short-circuiting state (arc burning state removed)
*(I=190A, $v_d$=5.2m/min, L=14mm, MS wire Ø1.2 mm, CP mode, $K_I$=60kA/s)*

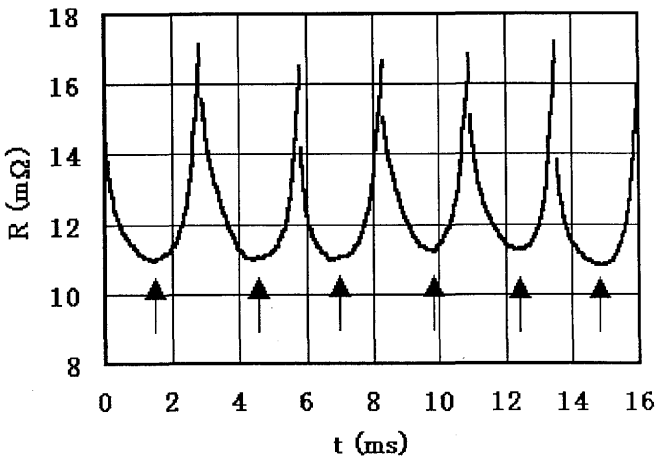


**Fig. 20** Resistance waveform in short-circuiting state
*(I=190A, $v_d$=5.2m/min, L=17mm, MS wire, Ø1.2 mm, CP mode, $K_I$=60kA/s)*

Its contribution to the total welding resistance becomes dominant. The measured value will depend more on the neck geometry *(~1/r²)* than on the wire length $L$ and so the total welding resistance will not correspond to the torch-to-workpiece distance.

A typical U-type resistance waveform automatically suggests picking the data in the centre part of the curve (see **Fig.20**). In this part the welding resistance reaches a local minimum with a first derivative equal to zero *(dR/dt=0)*. The arrows in the graph indicate appropriate points for wire resistance measurements. At these points both conditions are satisfied: the contact area is wide enough and the neck region is not significantly developed yet. Denoting the minimum welding resistance in a short-circuiting state by $R_{smin}$, the time when $R=R_{smin}$ by $t_{min}$, and ballast resistance in the measurement circuit by $R_{bal}$, the Eq.(2) can be rewritten as follows:

$$R_{s\min} = \int_0^L \frac{\xi(T(z,t_{\min}))}{S(z,t_{\min})} dz + R_{bal} \qquad (3)$$

The integral along the whole wire extension $L$ can be divided into liquid and solid parts :

$$R_{s\min} = R_{liq} + R_{sol} + R_{bal} \qquad (4)$$

where :

$$R_{liq} = \xi(T_d) \int_0^{L_d} \frac{1}{S(z,t_{\min})} dz \qquad (5a)$$

$$R_{sol} = \frac{1}{\pi r_w^2} \int_{L_d}^{L} \xi(T_o(z,t_{\min}))dz \qquad (5b)$$

assuming average temperature, $T_d$, in the liquid drop and temperature distribution, $T_o$, in the solid part of the wire.

The sensor, based on $R_{smin}$, will give appropriate signals, corresponding to torch-to-workpiece distance $L$, when $R_{liq}$ and $R_{sol}$ will not change significantly from one short-circuit to another. In other words when the liquid bridge profile $S(z)$ and temperature distribution $T_o(z)$ in the solid part of the wire at $t=t_{min}$ are not changed remarkably. As is indicated in the literature[29] both approximations are quite acceptable under most welding parameters and conditions.

The welding resistance in a short-circuiting stage reaches a minimum at $t_{min}\approx 1\text{-}2ms$. This time is long enough to create a stable and wide drop-pool contact. In the first moments of touching, the liquid bridge keeps the drop profile, except at a contact region close to the weld pool surface (see Fig.13 and **Fig.21**), where fast contact spreading occurs. As the resistance is integral (Eq.(5a)), small drop size variations will not produce significant welding resistance variations[29]. Larger drops are longer $L_d$, but they have larger cross-section $S$, too, and the variation effect will not be so crucial in this way.

Temperature distribution $T_o$ along the solid wire is discussed in Ref.[29]. It shows that as far as the wire temperature is concerned, the wire extension can be divided into 2 parts (see **Fig.22**). The first part, located close to the liquid-solid boundary, is significantly affected by a thermal conductive heat flow from the liquid drop to the solid wire. This part is relatively small.

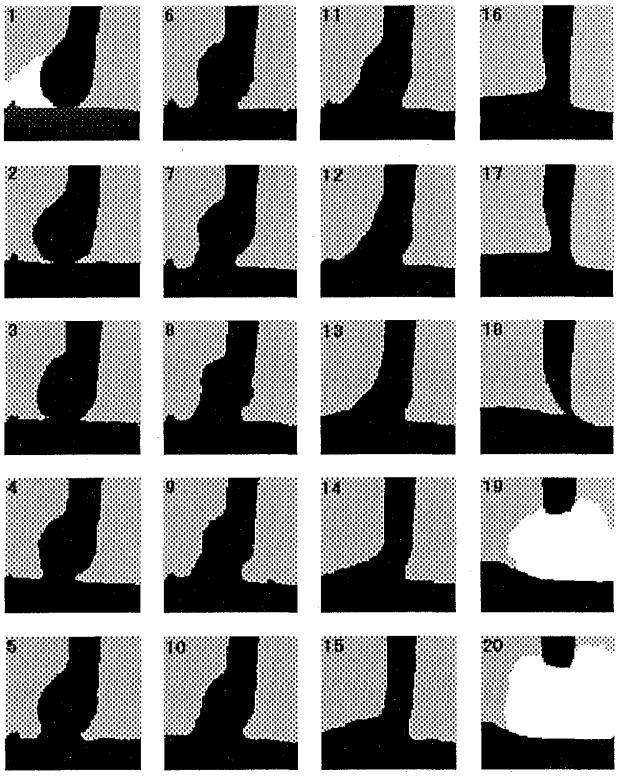


**Fig. 21** Liquid bridge profile development in GMAW/Ar (Δt=275μs)
*(I=150A, $v_d$=4.4m/min, L=15mm, MS wire, Ø1.2 mm, CP mode, $K_I$=60kA/s)*

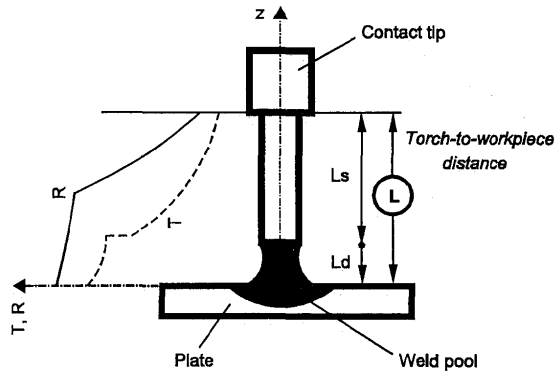


**Fig. 22** Schematic diagram of resistance and temperature distribution in MS wire after the contact stage

The thermal conduction term is less than 0.5% of Joule heat in regions ≈0.5-0.7 mm from the liquid-solid boundary. The 2nd cold part is located above the thermal conductive region. This part of the solid wire is heated only by Joule heating. The temperature distribution shows continuous decrease towards the welding tip with a typical temperature gradient ($\approx -10^4$ °C/m) for a mild steel wire. However, it can be found from Fig. 10 that the resistivity of mild steel is high when the temperature is above the Curie point ($\approx 800$°C). This indicates that wire regions close to the welding tip make small contributions to the total wire resistance. Similarly to the GMAW with spray transfer mode, temperature of the solid wire reaches a "quasistationary" temperature distribution, which does not follow rapid current changes, caused by a short-circuiting metal transfer ($\approx 100$Hz). This leads to the conclusion that the most important factors controlling the total wire resistance during a short-circuiting state are : the liquid bridge profile $S$ and the length of the solid wire with higher temperature $T \geq 800$°C.

**Figure 23** shows the welding resistance of 6 short-circuits from Fig.20 with similar durations. The short-circuit time was normalised to a dimensionless 0-100% scale. All curves show a typical U-type shape with very close minimum values of resistance $R_{smin} \approx 11 m\Omega$ in the centre part. Taking account all previous discussions the value $R_{smin}$ was selected as the sensor output for torch-to-workpiece detection. The sensor was tested under various welding parameters and conditions.

### 4.5 Through-the-wire sensor characteristics

Series of tests were carried out with mild steel and stainless steel wires at various values of welding current, voltage, torch height, short-circuit current slope, shielding gases, wire diameters, etc. Some downhill and uphill welding tests were performed, also.

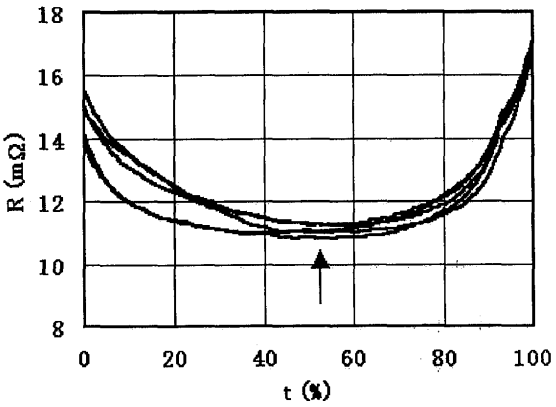


**Fig. 23** Resistance waveform in short-circuiting state
*(I=190A, $v_d$=5.2m/min, L=17mm, MS wire, Ø1.2 mm, CP mode, $K_I$=60kA/s)*

**Figure 24** shows the results of tests when torch-to-workpiece distance $L$ was gradually changed in a range from 8 to 23 mm. It is obvious from the graph that the sensor provides a stable signal of the torch position in spite of tremendous variations of instant welding parameters (see Fig.5). The torch-to-workpiece distance can be reliably extracted from the welding resistance signal. The bigger the torch-to-workpiece distance is, the higher the sensor signal level becomes.

The sensor signal shows some ripples. The ripples become higher as torch height increases. As the sensor detects the torch distance from the weld pool surface, the signal ripples are mostly generated by weld pool surface vibrations (reinforcements), drop size variations and violent touching-spot migration, which is extremely intensive mainly in GMAW with $CO_2$ shielding gas due to erratic drop repulsion. Experiments with various shielding gases, rich in Ar content (such as 100% Ar, mixture 80%Ar+20%$CO_2$) show that Ar stabilises the arc burning, drop growth and touching spot, and finally produces smaller ripples in the sensor output.

The ripples cause a torch-to-workpiece distance detection error. The average peak-peak amplitude of ripples is about 1mΩ and so the distance detection error

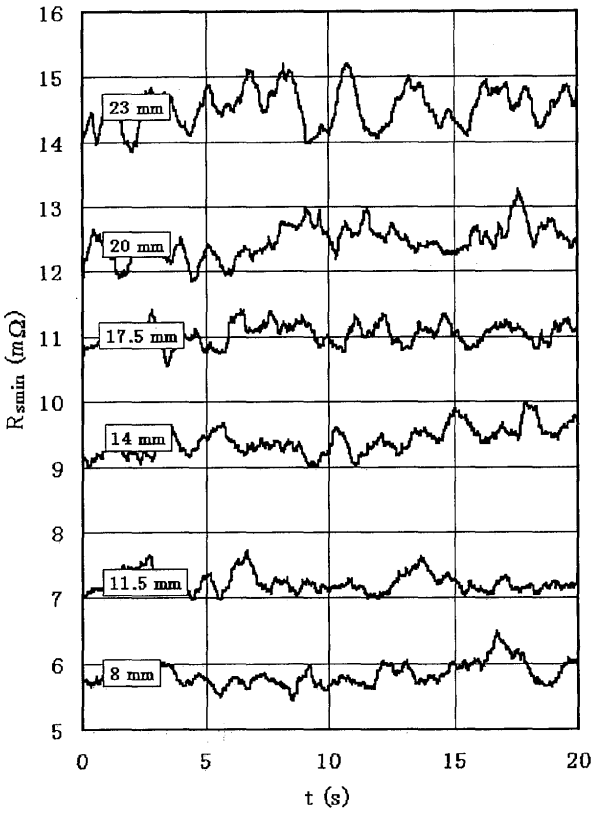


**Fig. 24** Waveform of sensor output at various torch-to-workpiece distances
*(I=165A, U=20V, L=8-23mm, $v_d$=4m/min, MS wire, Ø1.2 mm, CP mode, $K_I$=60kA/s)*

can be estimated ±0.8 mm. With typical value of wire extension about 16 mm, the estimation represents a relative error ±5%, which is quite acceptable tolerance.

**Figure 25** shows the sensor static characteristics. It is obvious from the graph that the sensor output $R_{smin}$ is sufficiently sensitive to the torch-to-workpiece distance $L$. Moreover the input-output function is linear in the stated range of torch height. For mild steel wire ∅1.2mm the sensor sensitivity $\Pi$ was 0.6 mΩ/mm. The linear

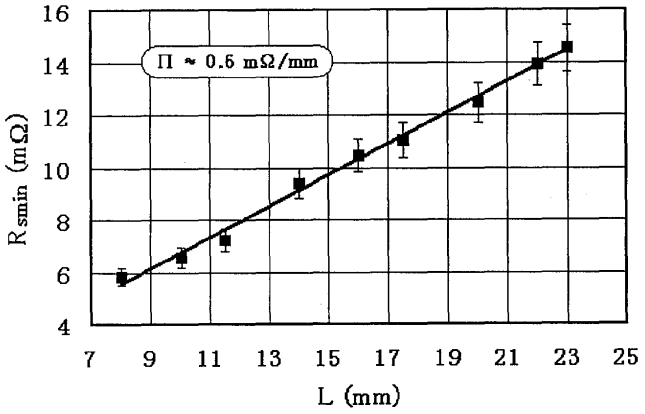


**Fig. 25** Sensor output vs. torch-to-workpiece distance *(I=165A, U=20V, L=8-23mm, $v_d$=4m/min, MS wire, ∅1.2 mm, CP mode, $K_I$=60kA/s)*

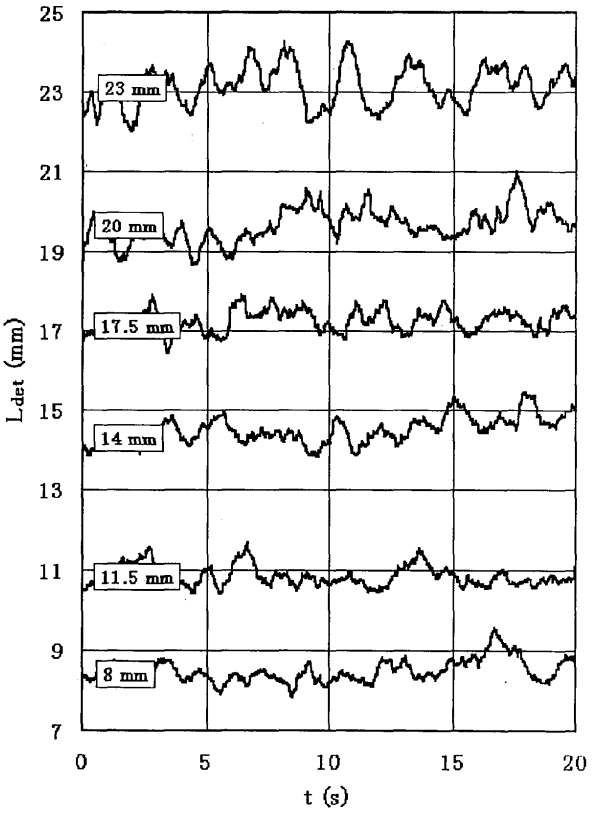


**Fig. 26** Torch-to-workpiece distance detection by means of through-the-wire sensor *(I=165A, U=20V, L=8-23mm, $v_d$=4m/min, MS wire, ∅1.2 mm, CP mode, $K_I$=60kA/s)*

input-output characteristics of the sensor indicate a "constant" wire resistance increase for wire length increase. For mild steel wire ∅1.2mm, the increase by 0.6 mΩ/mm corresponds to resistivity $\xi \approx 680\mu\Omega$/mm at equivalent temperature $T_{eqv} \approx 600°C$ (see Fig. 10).

**Figure 26** shows the torch-to-workpiece distance $L_{det}$ detected from the sensor signal be means of its static characteristics. At low torch height values the sensor accuracy can be estimated as ± 0.5mm, at higher values of torch height the sensor accuracy is reduced to ± 1mm.

To use the sensor in a feedback control, fast time response of the sensor is required. The through-the-wire sensor does not work continuously, but only in discrete intervals - during short-circuiting stages. **Figure 27** shows both a short-circuiting frequency and a measurement frequency for the sensor. The principle of the sensor requires a wide drop-pool contact, which is formed at $t > 1ms$. During the GMAW/$CO_2$ process there are some short-circuits with very short duration (see Fig.5). These short-circuits are not suitable for a torch-to-workpiece distance measurement. The sensor measurement frequency is less than the short-circuiting frequency in this way. The measurement frequency is in the range from 50 to 65 Hz.

Interest was also focused onto particular sensor signal stability under various welding parameters and conditions. It is generally known that particular welding parameters and conditions have a substantial effect on short-circuiting phenomena of the welding process.

**Figure 28** shows a short-circuit duration distribution when welding voltage is changed from 19V to 25V. The significant effect of the welding voltage is evident. At U=19V the distribution is very wide. Both short and long short-circuits can be observed in the process. On the other hand when the welding voltage is set to 25V, only very short durations can be found.

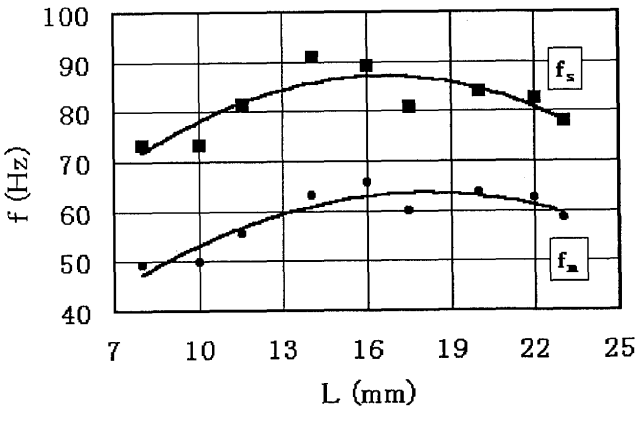


**Fig. 27** Short-circuiting ($f_s$) and measurement ($f_m$) frequency of the through-the-wire sensor in GMAW/$CO_2$ *(I=165A, U=20V, L=8-23mm, $v_d$=4m/min, MS wire, ∅1.2 mm, CP mode, $K_I$=60kA/s)*

**Figure 29** shows the dependency of short-circuit duration, short-circuit frequency and measurement frequency of the sensor on welding voltage. All parameters are strongly affected by the welding voltage. The higher the voltage $U$ is set, the lower values $t_s$, $f_s$ and $f_m$ are observed. When welding voltage is changed from 19V to 25V the short-circuit duration is reduced 4 times (from 4 to 1 ms) and short-circuit frequency decreases from 60 to 35 Hz. The measurement frequency is significantly reduced from 40 to 12 Hz. The torch height can be detected only 12 times per second in this way. Regardless of these changes, the sensor output is stable, not significantly affected by the welding voltage (see **Fig.30**).

Welding power source dynamics also have a significant effect on the GMAW/$CO_2$ process. **Figure 31** shows dependency of short-circuit duration $t_s$ on the power source current slope $K_I$. When the short-circuit current slope is increased the short-circuit duration distribution dramatically moves to shorter duration values. When slow current rise of the power source is set ($K_I \approx 31\text{-}54$ *kA/s*) both short and long durations can be found. The welding process is very unstable and irregular metal transfer can be detected. At very low

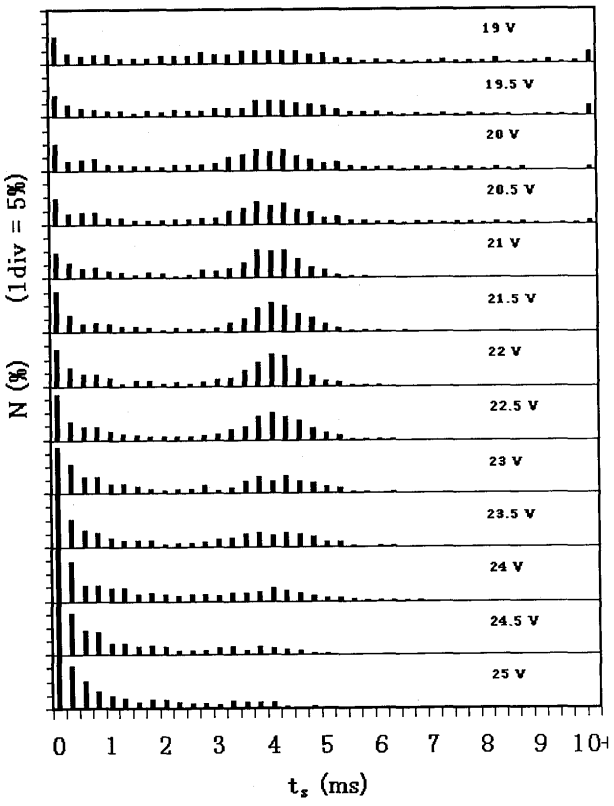


**Fig. 28** Distribution of short-circuiting duration ($t_s$) at various welding voltage values
*(I=190A, U=19-25V, L=14mm, $v_d$=5.2m/min, MS wire, Ø1.2 mm, CP mode, $K_I$=60kA/s)*

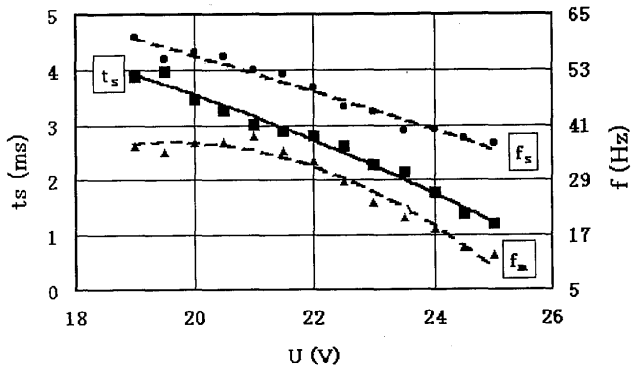


**Fig. 29** Short-circuit duration ($t_s$) and frequency ($f_s$) and sensor measurement frequensy ($f_m$) vs. welding voltage (U)
*(I=190A, U=19-25V, L=14mm, $v_d$=5.2m/min, MS wire, Ø1.2 mm, CP mode, $K_I$=60kA/s)*

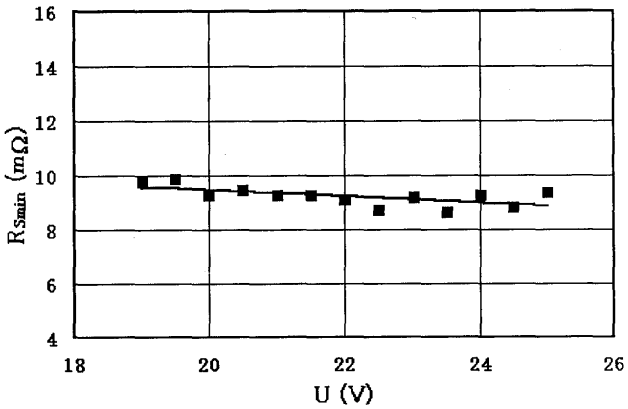


**Fig. 30** The sensor output ($R_{smin}$) vs. welding voltage (U)
*(I=190A, U=19-25V, L=14mm, $v_d$=5.2m/min, MS wire, Ø1.2 mm, CP mode, $K_I$=60kA/s)*

values ($K_I \approx 31\text{-}33$ *kA/s)* the number of very long short-circuits with $t_s \geq 10ms$ represent a relatively high portion (≈15%) and the distribution peak (the most probable short-circuit duration) is at about $t_s$=*5ms*. Higher power source dynamics will dramatically reduce the number of long short-circuit duration. At current slope $K_I \approx 100\text{-}200$ *kA/s* the distribution peak moves to 2 ms and long duration values disappear.

**Figure 32** shows a strong effect of $K_I$ on process characteristics. When the current slope is increased from 31 to 200kA/s the short-circuit duration $t_s$ is decreased almost 6 times, from 6 to 1 ms. The short-circuiting frequency is in the range 30-75Hz and the measurement frequency from 15 to 60 Hz.

In spite of significant changes in metal transfer characteristics, the sensor provides a relatively stable signal for torch height detection. (see **Fig. 33**). The signal depends slightly on the current slope. The bigger the slope $K_I$ is, the higher the sensor signal becomes. From the graph in Fig. 32 it can be seen that the average value of short-circuit duration is $t_s$<*2ms* when the

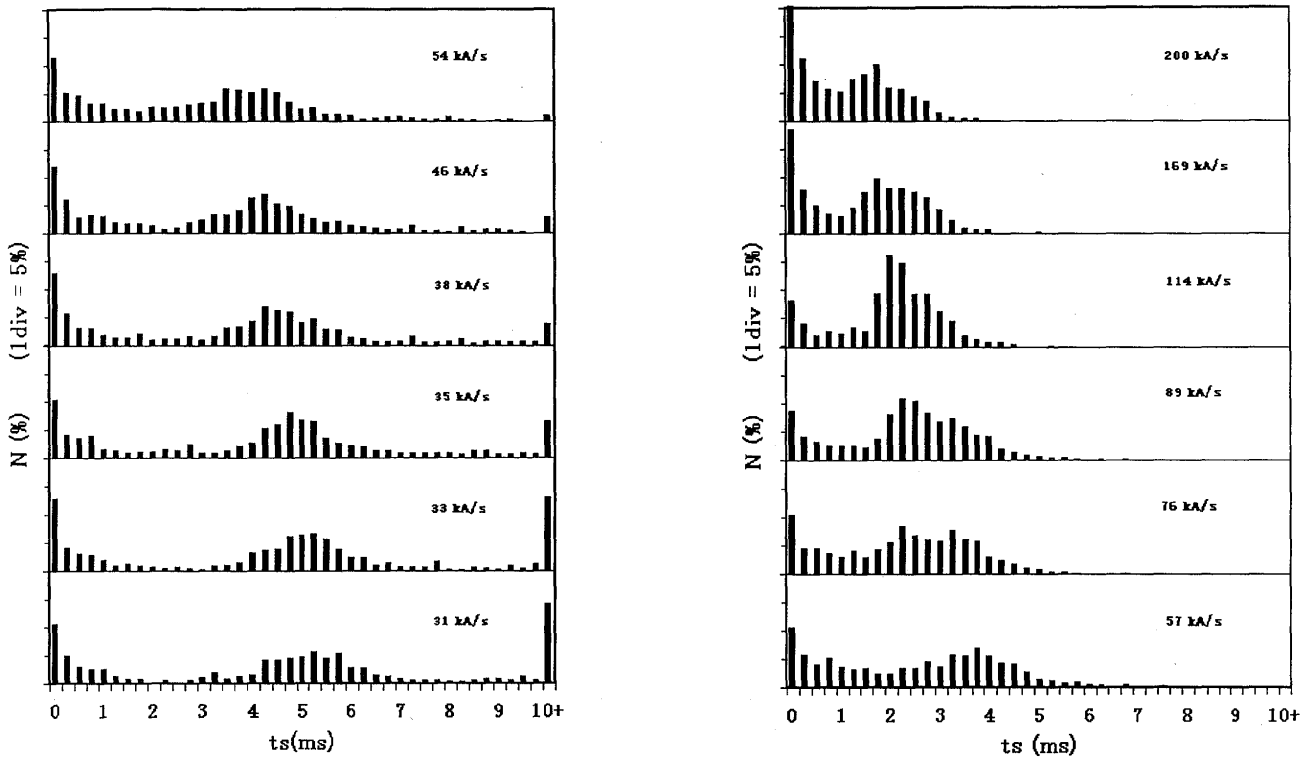


**Fig. 31** Distribution of short-circuiting duration ($t_s$) at various short-circuit current slopes ($K_I$)
*(I=175A, U=20.5V, L=14mm, $v_d$=5.2m/min, MS wire, Ø1.2 mm, CP mode, $K_I$=31-200kA/s)*

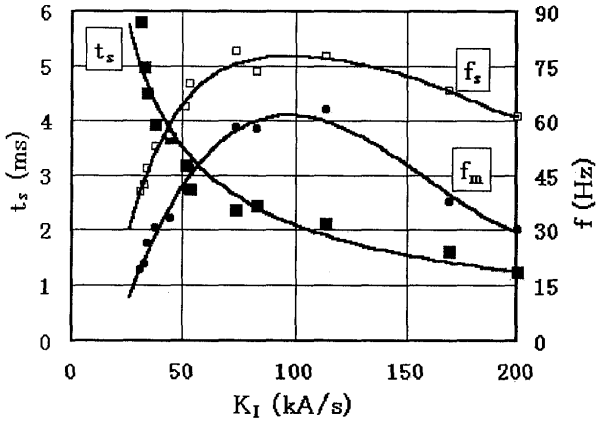


**Fig. 32** Short-circuit duration ($t_s$) and frequency ($f_s$) and sensor measurement frequency ($f_m$) vs. current slope ($K_I$)
*(I=175A, U=20.5V, L=14mm, $v_d$=5.2m/min, MS wire, Ø1.2 mm, CP mode, $K_I$=31-200kA/s)*

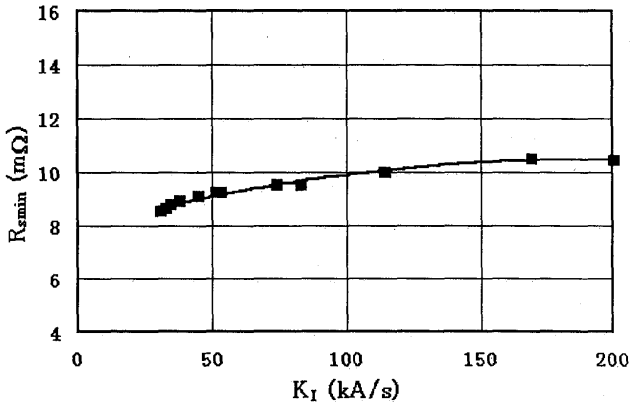


**Fig. 33** The sensor output ($R_{smin}$) vs. current slope ($K_I$)
*(I=175A, U=20.5V, L=14mm, $v_d$=5.2m/min, MS wire, Ø1.2 mm, CP mode, $K_I$=31-200kA/s)*

current slope is $K_I$>100kA/s. This indicates the fact that when $K_I$>100kA/s the drop-pool contact is not wide enough and the liquid bridge is already squeezed by electromagnetic forces. The rapid short-circuiting current ramp generates very intensive squeezing force too early. The total welding resistance is strongly affected by high resistance of contact and neck regions.

**Figure 34** shows the sensor output $R_{smin}$ as a function of short-circuit duration $t_s$. This shows that in the region where $t_s$< 2ms the sensor output $R_{smin}$ becomes higher with decrease values of $t_s$. It confirms assumption discussed above, that during short short-circuiting duration ($t_s$<2ms) there is not enough time to form a wide and stable drop-pool contact. The contact area is small and the bridge already becomes squeezed by electromagnetic forces due to high welding currents. Both contact and neck locations represent high resistance regions, which finally lead to increases of the total welding resistance and higher sensor outputs.

**Figures 35** and **36** document the sensor signal $R_{smin}$ in GMA/$CO_2$ welding, when torch-to-workpiece distance $L$

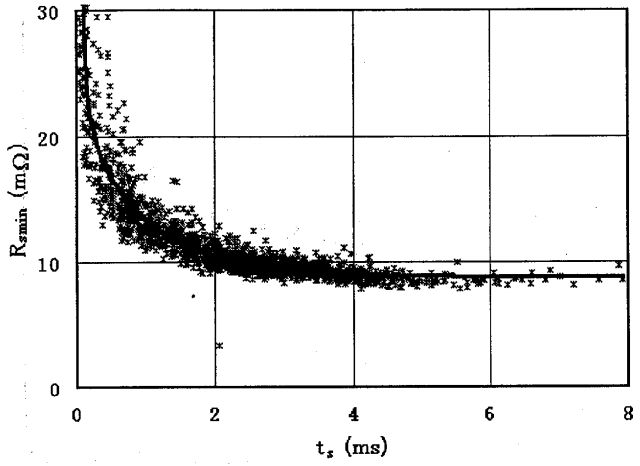


**Fig. 34** Sensor output ($R_{smin}$) vs. short-circuit duration ($t_s$)
*(I=160A, U=20V, $v_d$=5.2m/min, L=14mm, MS wire Ø1.2 mm, CP mode, $K_I$=60kA/s)*

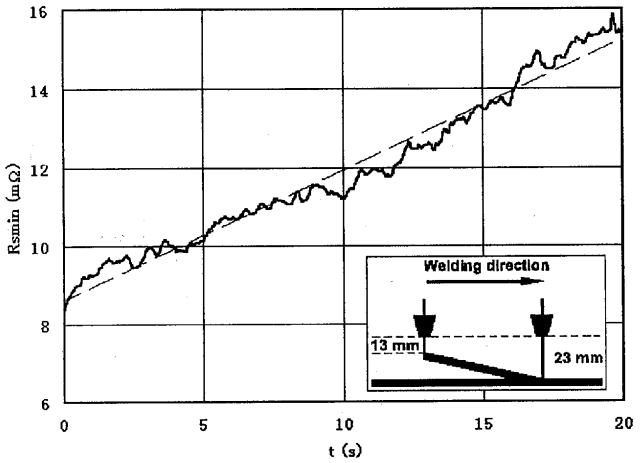


**Fig. 35** Sensor output during downhill welding
*(I=180A, U=19V, $v_d$=5.2m/min, L=13-23mm, MS wire Ø1.2 mm, CP mode, $K_I$=60kA/s)*

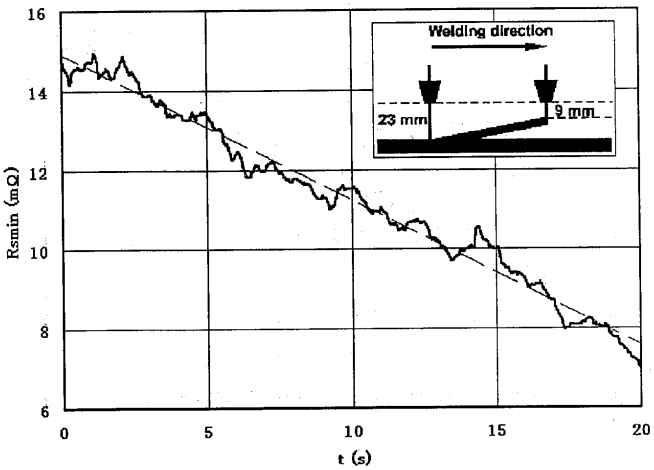


**Fig. 36** Sensor output during uphill welding
*(I=180A, U=19V, $v_d$=5.2m/min, L=9-23mm, MS wire Ø1.2 mm, CP mode, $K_I$=60kA/s)*

is continuously changed. In both experiments the welding speed was 5.3 mm/s. In downhill test the torch height $L$ was increased from 13 to 23 mm. The graph indicates a sensor output from 8.5 to 15.5 mΩ. From the sensor calibration characteristics (Fig.25) the detected torch-to-workpiece distance $L_{det}$ is in a range 12.5-23.5 mm. The values detected by means of sensor $L_{det}$ are very close to real torch-to-workpiece values $L$.

In uphill test (Fig.36) the torch-to-workpiece distance changed linearly from 23 to 9 mm. The sensor output gradually decreased from 14.5 to 7 mΩ and corresponding torch height $L_{det}$, measured by the sensor, reduced from 22.5 to 10 mm. The values are again very close to real values $L$.

A small difference (≈1mm) between uphill and downhill sensor values were caused by a different weld bead formations in the welding tests. The weld bead reinforcement difference was detected by the sensor as the sensor principle is exactly based on torch-to-pool distance measurement techniques.

## 5. Conclusions

A study of short-circuiting metal transfer in GMAW, based on numerical modelling of heat flow in moving electrodes, experimental observations of liquid bridge profile in simulated homophase drop-pool touching experiments, qualitative analysis of short-circuiting metal transfer phenomena in GMAW by means of high speed video and precise measurements of welding parameters have led to some new conclusions, which can be summarised as follows:

(1) In GMAW with a short-circuiting metal transfer mode, similar to that spray transfer mode, temperature in solid wire extension reaches a quasi-stationary distribution, except in the immediate vicinity of the molten drop at the wire tip.

(2) When a mild steel wire is used, the resistance of the solid part with low temperature (below the Curie point ) is relatively small in comparison with that of a solid part with high temperature and a liquid bridge.

(3) In the homophase drop-pool touching process, three typical stages can be identified : drop-pool contact formation, liquid transfer and neck squeezing (when bridge breakage occurs). Due to a small cross-section area of the contact/neck region at the beginning/end of the bridging process the liquid bridge resistance has a typical **U**-type shape profile in time.

(4) When high resistivity welding wires are used ( e.g. mild steel, stainless steel, etc.), the welding resistance can be used for short-circuiting phenomena monitoring.

(5) Due to a strong electromagnetic force, generated by high welding current, the neck squeezing stage duration is similar to the contact formation stage duration, resulting in more-less symmetrical U-shape profile of welding resistance during a short-circuiting state.

(6) The short-circuit welding resistance can be used for torch-to-workpiece distance detection in GMAW with short-circuiting metal transfer mode. The through-the-wire sensor, based on a minimum value of short-circuit welding resistance, provides a reliable torch-to-workpiece distance signal for a feedback control in seam tracking systems.

**Acknowledgements**

The authors are grateful to Prof. M. Ushio and Dr. T. Ueyama from R&D division of Daihen Corp. for technical support of the research project.

**References**

1) Cook, G.E. : Feedback and Adaptive Control in Automatic Arc Welding Systems, Metal Construction, 9, 1981, p.551.
2) Flasskamp, H.:Volltransistorisierter Stromquelle Multitig, Trennen+Fugen, 7, 1980, p.65.
3) Cook,G.E. : Direct Current Power Supply, US Patent, 389 628 7, 222, 1975.
4) Arata,Y. : New Perfect Automatic Control System for Arc Welding, Doc. IIW XII-K-6-71, 1971, p.11.
5) Takeuchi,N. : Some Types of Wire Ground Sensor, In : Sensors and Control Systems in Arc Welding, Chapman & Hall Pub., 1994, p.285-291.
6) Masumoto, I., Nomura,H. : Development and Application of Sensors and Sensor Systems for Arc Welding in Japan, Doc. IIW XII-C-031-82, 1982, p22.
7) Heitmayer,U., Weman,K. : Adaptive Sensing : Key to the Adult Robot, Welding and Metal Fabrication, 12, 1981, p.592-596.
8) Nomura,H. et al : Automatic Welding of the Corrugated Membrane of an LNG Tank, Metal Construction, 7, 1982, p.391-395.
9) Towata,T. : Outline and Its Application of Shin Meiwa of Sensorless Sensing System, Robot, 25, 1979, p.16-20.
10) Fukuoka,H. : Application of a Touch Sensor to an Arc Welding Robot, In : Sensors and Control Systems in Arc Welding, Chapman&Hall Publishing, London, 1994, p.292-299.
11) Nomura,H. : Sensors and Control Systems in Arc Welding, Chapman&Hall Publishing, London, 1994, p.40-43.
12) Fujimura,H., Ide,E., Inoue,H. : Joint Tracking Control Sensor of GMAW, Trans. JWRI, 1, 1987, p.32-40.
13) Nomura,H., Sugitani,Y. Mutayama,M. : Development of Automatic Fillet Welding Process with High Speed Rotating Arc, Trans. JWRI, 2, 1987,p.26-34.
14) Orszagh,P., Sencak,V. Adaptive Control of Torch Position with Arc Sensor, IIW Doc SG 212-763-90.
15) Ushio,M., Mao,W. : Modelling and Characteristics of Through-the-arc sensor, Trans. JWRI, 1, 1994, p.13-19.
16) Dilthey,U., Stein,L., Oster,M. : Through-the-arc Sensing - An Universal and Multipurpose Sensor for Arc Welding Automation, JOM, 1, 1996, p.6-12.
17) Arata,Y., Inoue,K. : Application of Digital Picture Processing Technique to Automatic Control, Doc. IIW XII-K-65-76, 1976, p.15.
18) Pan,J.L., Wang,J.L. : Development of Two-directional Seam Tracking System with Laser Sensor, Welding Journal, 2, 1983, p.28.
19) Drews,P., Starke,G. : Development Approaches for Advanced Adaptive Control in Automated Arc Welding Proc. IIW International Conference, Pergamon Press, Oxford, 1985, p.115-124.
20) Orszagh,P., Vyjidak,O. : System for Feedback Control of Circumferential TIG Welding of Pipes, Proceeding of Advanced Welding Systems, London, 1985.
21) Boillot,J.P., Yu,X., Fontaine,J.C.: Automatic Welding Using 3D Laser Vision System, Welding in the World, 1994, p.173-182.
22) Ushio,M., Mao,W. : Sensors for Arc Welding : Advantages and Limitations, Trans. JWRI, 2, 1994, p.135-141.
23) Technical Commission on Welding Process of JWS : Sensors and Control Systems in Arc Welding, Kuroki Publish., 1991.
24) By,J., Kim,W., Na,J. : A Study on an Arc Sensor for Gas Metal Arc Welding of Horizontal Fillets, Welding Journal Supplement, 8, 1991, p.216s-221s.
25) Ushio,M., Liu,W., Mao,W. : An Experimental Investigation of Dynamic Behaviour of Arc Sensor in GMAW in Short Circuit Transfer Mode, Trans. JWRI, 1, 1995, p.25-30.
26) Gonzales,R.C., Wintz,P. : Digital Image Processing, Addison-Wesley publishing, London, 1977.
27) Huang, ,T.S. : Picture Processing and Digital Filtering, in Topics in applied physics, Springer publishing, 2nd edition, New York, 1979
28) Mao,W. : Dynamic Characteristics of Through-the-arc Sensor in GMAW, PhD Thesis, JWRI, Osaka University, 1997
29) Orszagh,P., Kim,Y.C., Horikawa,K. : Simulation of Wire Heating in GMAW with Short-circuiting Metal Transfer, Trans. of JWRI (27), 2, 1997, (in print).
30) Kaiser,J.G., Dunn,G.J., Eagar,T.W. : The Effect of Electrical Resistance on Nugget Formation during Spot Welding, Welding Journal, 6, 1982, p. 378s-385s.
31) Thornton,P.H., Krause,A.R., Davies, R.G. : Contact Resistance in Spot Welding, Welding Journal, 12, 1996, p.402s-412s.

*Symbols*

*Greek letters*

$\Pi$ sensor sensitivity
$\rho$ mass density
$\sigma$ surface tension
$\xi$ wire resistivity
$\phi$ wire diameter

*Vectors*

$H$ stabiliser setting parameters
$X$ welding process input parameters
$Y$ welding process output parameters
$W$ welding process/system perturbations
$U$ welding system setting parameters
$Q$ adaptive welding quality parameters

*Roman letters*

$f_m$ measurement frequency of the sensor
$f_s$ short-circuiting frequency
$g$ gravity constant
$I$ welding current
$K_I$ dynamic characteristics of the power source ($K_I = dI/dt$)
$K_U$ static characteristic of the power source ($K_U = \Delta U/\Delta I$)
$L$ torch-to-workpiece distance
weld pool is part of the workpiece
torch bottom is the bottom end of contact tip
$L_a$ arc length
$L_d$ liquid drop length
$L_{det}$ $L$ detected by the sensor
$L_e$ wire extension ($L_e=L_s+L_d$)
$L_s$ solid wire length extension
$L_t$ typical length of the liquid
$N$ number of occurrence (counts)
$r$ radius
$r_c$ contact radius
$r_n$ neck radius
$r_w$ radius of the solid wire
$R$ resistance
$R_b$ bridge resistance
$R_{bal}$ ballast resistance
$R_{cyl}$ resistance of cylinder
$R_{liq}$ resistance of liquid bridge
$R_{smin}$ minimum resistance in short-circuiting state
$R_{sol}$ resistance of solid wire
$S$ cross-section of the wire/bridge ($S=\pi r^2$)
$t$ time
$t_a$ arc burning duration
$t_{min}$ time at minimum resistance
$t_s$ short-circuiting duration
$T$ temperature
$T_d$ drop temperature
$T_{eqv}$ constant temperature equivalent to $T_o$
$T_o$ temperature profile in solid wire
$U$ welding voltage
$v_d$ wire feeding rate
$z$ wire axis from weld pool to torch tip

*Special symbols*

$\underline{x}$ average value of $x$

*Abbreviation*

| | |
|---|---|
| *ACC* | automatic current control |
| *AVC* | automatic voltage control |
| *A/D* | analog/digital converter |
| *D/A* | digital/analog converter |
| *DMA* | direct memory access |
| *CC* | constant current mode |
| *CP* | constant potential mode of the power source |
| *GMAW* | gas metal arc welding |
| *GMA/$CO_2$* | GMAW in $CO_2$ shielding gas |
| *HSRA* | high speed rotating arc technique by NKK Corp. |
| *MS* | mild steel MIX-50S |
| *SS* | stainless steel YT-308T |